



Regular Article

Grain size effect on radiation tolerance of nanocrystalline Mo

G.M. Cheng^a, W.Z. Xu^a, Y.Q. Wang^b, A. Misra^c, Y.T. Zhu^{a,*}^a Department of Materials Science and Engineering, North Carolina State University, Raleigh, NC 27695, USA^b Materials Science and Technology Division, Los Alamos National Laboratory, Los Alamos, NM 87545, USA^c Department of Materials Science and Engineering, University of Michigan, Ann Arbor, MI 48109, USA

ARTICLE INFO

Article history:

Received 28 March 2016

Received in revised form 30 May 2016

Accepted 8 June 2016

Available online 16 June 2016

Keywords:

Radiation damage

Body-centered cubic (bcc)

Nanocrystalline

Grain size effect

Magnetron sputtering

ABSTRACT

We report a significant grain size effect on radiation tolerance of nanocrystalline Mo under He ion irradiation. Irradiation-induced dislocation loops mainly contribute to the irradiation-induced hardening of Mo films with grain size of >90 nm, while few such loops in those with grain size of <90 nm. The hardness increment after irradiation decreases with decreasing the grain size, and approaches zero at the grain size of 25 nm. Also, the size and the density of irradiation-induced He bubbles decrease as the grain size decreases. This observation provides direct evidence that nanocrystalline body-centered-cubic metals have greater radiation tolerance than their ultra-fine-grained or coarse-grained counterparts.

Published by Elsevier Ltd.

Radiation damage is one of the critical issues for developing advanced materials used in next generation nuclear plants [1–8] and spacecrafts [9]. Hardening, swelling, embrittlement and creep are some of the critical issues associated with radiation damage. Irradiation can induce interstitials, vacancies or He bubbles in microstructure, which will further agglomerate to form loops, interstitial or vacancy clusters and voids in materials [10,11]. Formation of voids will lead to swelling and embrittlement, which are the main cause of material failure under irradiation environment [12]. Therefore, how to control the generation of irradiation-induced defects and mitigate the negative effects of He bubbles is the key to design advanced radiation tolerant materials with a balance of mechanical and thermal properties [2,13].

Body-centered cubic (bcc) metals and alloys have attracted much attention in the past decade due to their reduced-activation under irradiation environment [14–18]. The studies on the oxide-dispersion strengthened (ODS) ferrite steels [19–22] have showed great radiation tolerance since dispersed nanoparticles in the matrix increase the volume fraction of the interfaces which can act as sinks for irradiation-induced defects, especially for He bubbles.

Similarly, nanocrystalline (NC) materials exhibit great potential for such applications because a large fraction of grain and interphase boundaries can act as effective sinks for irradiation-induced vacancies and bubbles [2,6,23,24]. Refining the grains of materials into nanometer size can significantly alter the physical, chemical and mechanical behaviors of the materials [25–31]. Previous reports [32–35] on fcc/bcc nanolayered composites have showed extreme tolerance to He bubbles,

which are prone to segregate at interphase boundaries. Bulk NC metals have also displayed extraordinary radiation healing behavior due to grain boundary (GB) accommodation of defects [36–38].

Although there are many reports about the radiation damage on NC metals and alloys, it remains elusive about how the change of grain size affects the radiation tolerance. To explore this issue, here we investigate the effect of grain size on the mechanical properties and the microstructure evolution of NC bcc metals before and after He ion irradiation, using Mo as a model material.

Mo films with thickness of at least 1.5 μm were synthesized on silicon (100) substrates using magnetron sputtering. The deposition rate was varied in order to control the average grain size. Mo films with average grain sizes ranging from 25 to 455 nm and coarse-grained (CG) Mo foil (listed in Table 1) were irradiated together at room temperature, using 200 keV He ions with a total fluence of 1.4×10^{17} ions/cm². The peak damage was ~4 dpa (displacement per atom) and the He concentration ~1.9% (see details in the supplementary materials). The indentation hardness and modulus of Mo samples before and after He ion irradiation were measured based on an average value of at least 9 indents at each load from HYSITRON T1900 TriboIndenter with a Berkovich tip (tip diameter, 45 nm). The maximum indentation depth was 150 nm for all thin film specimens and 250 nm for bulk specimen. Microstructures of Mo samples before and after irradiation were examined by X-ray diffraction, scanning electron microscopy (SEM) and transmission electron microscopy (TEM). Both plane-view (peeling off) and cross-section (wedge-shaped) samples were ion-milled at –70 °C, with low energy (3.5 keV) and low angle (<4°). TEM and high-resolution TEM (HRTEM) observations were carried out using a JEOL 2010F microscope operating at 200 kV.

* Corresponding author.

E-mail address: ytzhu@ncsu.edu (Y.T. Zhu).

Table 1

Average grain size (from plane-view) corresponding to the different samples from Mo thin films prepared by magnetron sputtering and as-received Mo foil.

Sample type	Average grain size (nm)
Mo6	25
Mo5	44
Mo4	68
Mo3	90
Mo2	185
Mo1	455
Mo0	3900

Series of Mo films with different average grain size were prepared, and the grain size distribution was uniform based on both plane-view and cross-sectional TEM observations. Fig. 1 shows the morphologies of one of the typical NC Mo films. The thickness of the Mo film was measured to be 1.5 μm from the cross-sectional view in Fig. 1d obtained by SEM. From the plane-view bright-field and dark-field TEM images in Fig. 1b and c, the distribution of the grain size is uniform (see the plot in the inset of Fig. 1b), and the average grain size is 44 nm, taken 500 grains into account. The average grain size along the growth direction is 100 nm, as shown in Fig. 1e and f.

The hardness deviation of bcc Mo samples before and after He ion irradiation is presented in Fig. 2a as a function of the grain size, where the grain size is the average value of each Mo sample (Table 1). The reduction of grain size introduces strong hardening in NC Mo thin films before He ion irradiation (marked by open square in Fig. 2a), which is similar to the previous report [30]. The hardness of Mo samples after irradiation continuously increases with decreasing the grain size. And the hardness values of irradiated Mo samples (marked by open circle in Fig. 2a) are larger than those of their unirradiated counterparts. It indicates that there is additional irradiation-induced hardening due to the irradiation-induced defects, besides of the hardening from the reduction of grain size. Note that there is no obvious change of grain size or residue stress of the Mo samples before and after He ion irradiation based on the XRD analysis. It can be seen from Fig. 2a that dramatic irradiation-induced hardening is in the irradiated samples with grain size of >90 nm.

Especially in CG Mo, the hardness of irradiated sample is increased by 4.5 GPa and reaches to 7.2 GPa, which means that a high density of defects is induced into the sample during He ion irradiation. However, the hardness increment ($\Delta H_{\text{ir}} = H_{\text{irradiated}} - H_{\text{unirradiated}}$) before and after irradiation decreases as the grain size decreases, shown in Fig. 2c (the hardness increment as a function of the grain size). The hardness increment has a dramatic decrease when the grain size is <90 nm, and is close to zero in NC Mo with a grain size of 25 nm. This is probably due to a remarkable reduction of irradiation-induced defects in them. Accordingly, the irradiation-induced hardening can be effectively reduced by decreasing the grain size.

Figs. 3 and 4 show the dominant irradiation-induced defects (He bubbles and dislocation loops) in irradiated NC and CG Mo with grain sizes of 44 nm (Mo5) and 3.9 μm (Mo0), respectively. It is clearly seen in Fig. 3a and c that both have a very high density of He bubbles, which is of the order of 10^{23} – 10^{24} m^{-3} (the number of bubbles per unit volume), but the distribution of He bubbles is different as the grain size changes. The He bubbles tend to segregate to the GBs in irradiated NC Mo (Fig. 3a). Note that the two TEM images are under the same imaging conditions. The density of He bubbles in irradiated NC Mo is less than that in irradiated CG Mo based on the statistic data in Fig. 2b, and the average diameter of He bubbles in irradiated NC Mo (Mo5) is 0.6 nm, which is only half of that in irradiated CG Mo (Mo0) with a value of 1.2 nm, shown in Fig. 3b and d.

Furthermore, there is a high density of dislocation loops in irradiated CG Mo ($\sim 10^{24} \text{ m}^{-3}$, the number of loops per unit volume), but less dislocation loops (10^{22} m^{-3}) in irradiated NC Mo, shown in Fig. 2d. Fig. 4 shows TEM and HRTEM images of the irradiation-induced dislocation loops in NC (Mo5) and CG (Mo0) Mo after He ion irradiation. Details of loop characterization (type, Burgers vector, etc.) in irradiated bcc bulk metals can be referred to Refs [39–41]. The irradiation-induced dislocation loops show clear image contrast in irradiated CG Mo (Fig. 4c) but not in irradiated NC Mo (Fig. 4a). A magnified TEM image of the dislocation loops in irradiated CG Mo is shown in the inset in Fig. 4c. And the edge-on interstitial loops in irradiated NC and CG Mo are marked in the HRTEM images in Fig. 4b (the inset) and d, respectively. Note that there is much less dislocation loops ($< 10^{20} \text{ m}^{-3}$) in all unirradiated Mo samples (see Fig. S3 in the supplementary materials). Moreover,

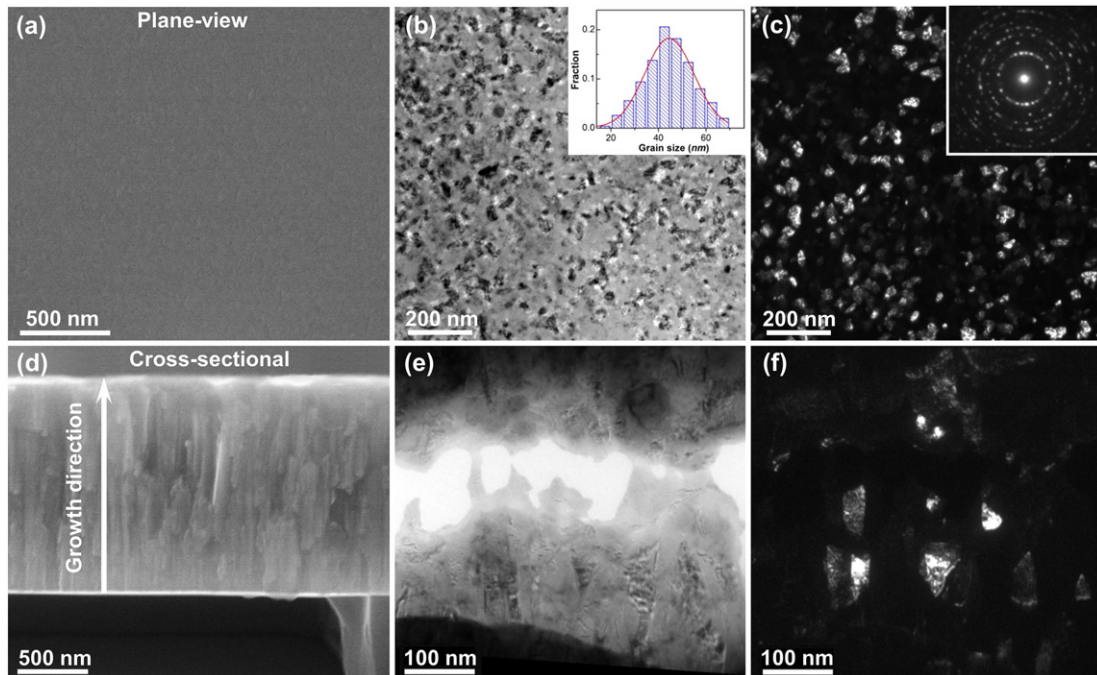


Fig. 1. SEM (a, d), bright-field TEM (b, e) and dark-field TEM (c, f) images of typical NC Mo film prepared by magnetron sputtering. (a–c) from plane-view; (d–f) from cross-sectional view. The inset in (b) shows the distribution of grain size based on 500 grains. The average grain size is 44 nm. The inset in (c) is the corresponding SAED pattern.

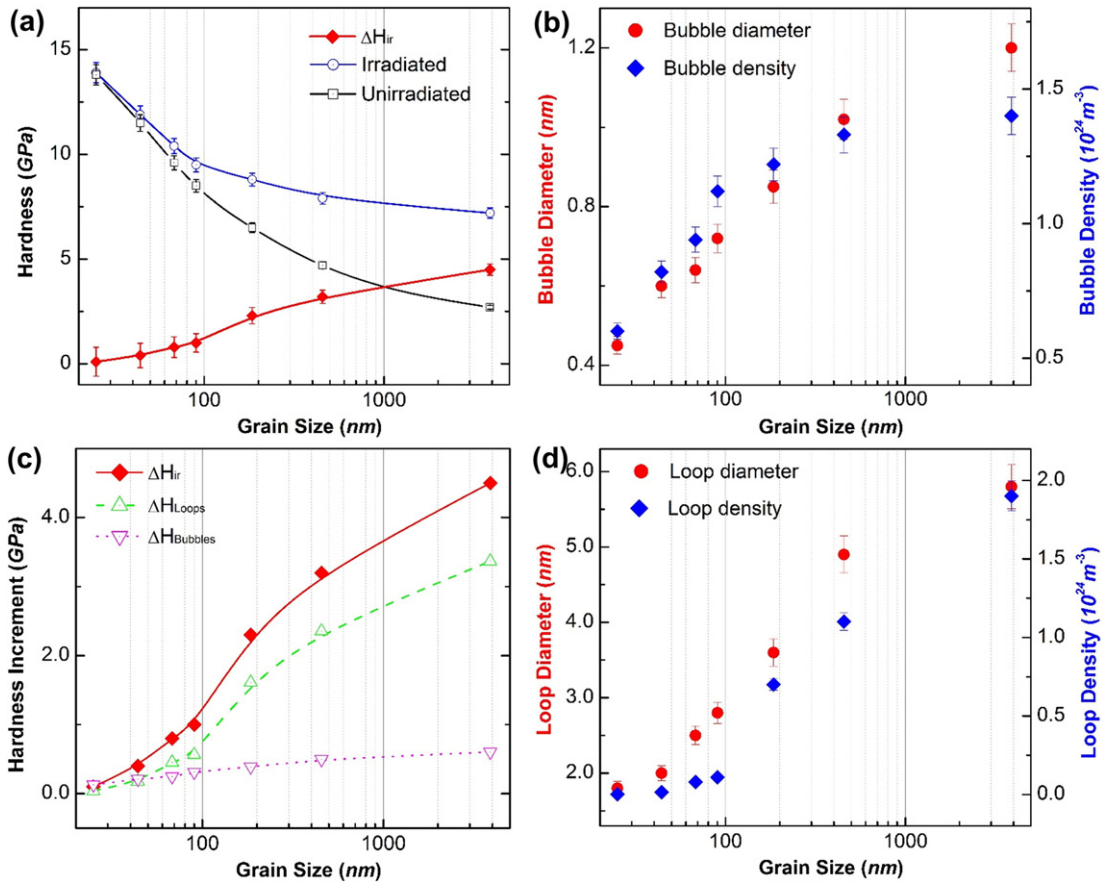


Fig. 2. Grain size effect on the hardening behavior of bcc Mo before and after He ion irradiation. (a) Hardness deviation of bcc Mo samples before and after irradiation; (c) Hardness increment after irradiation. (b, d) Distribution of size and density of irradiation-induced He bubbles and dislocation loops in bcc Mo samples after irradiation, respectively.

HRTEM investigation also revealed that there was a high density of dislocations with edge component in both irradiated NC and CG Mo (almost the same order of magnitude, $\sim 10^{15} m^{-2}$, the number of dislocations per unit area), shown in Fig. 4b and d. The observed dislocations in NC Mo were mainly from the edge or mixed dislocations [29,42] and their density was almost at the same order of magnitude in both irradiated and unirradiated samples. But most of them in irradiated CG Mo might be from the projection of dislocation loops since no obvious dislocation line was observed via two-beam imaging. Accordingly, irradiation-induced bubbles and dislocation loops may significantly contribute to the obvious irradiation-induced hardening phenomena in irradiated Mo samples with different grain size. In the following we will discuss the possible hardening mechanism from the irradiation-induced defects (He bubbles and dislocation loops) based on the statistical data in Fig. 2b and d.

As we know, irradiation-induced hardening is mainly related to the induced defects such as point defects, clusters, dislocations, loops and He bubbles. Here, the hardening effect can be divided into two parts [12]. One is from He bubbles, and the other is from dislocation loops, etc. For He bubble induced hardening, a hardening relationship developed by Friedel-Kroupa-Hirsch (FKH) [43,44] can be used to describe the irradiation-induced increase in yield strength, $\Delta\sigma_{bubble}$.

$$\Delta\sigma_{bubble} = \frac{1}{8}MGBdN_{He}^{2/3} \quad (1)$$

where M is Taylor factor, 3.05 for bcc metal; G is the shear modulus (GPa), ~ 128 GPa from the nanoindentation data; b is the Burgers vector (nm), $\frac{1}{2}\langle 111 \rangle$ used here; d is the bubble diameter (nm) and N the bubble density (m^{-3}). The increase in yield stress from FKH model corresponds to a hardness increase ($\Delta H_{bubble} \approx 3\Delta\sigma_{bubble}$) in Fig. 2c. As

shown, the hardening from He bubbles (marked by down triangle in Fig. 2c) is slightly decreased as the grain size decreases, but is much smaller than the total hardness increment (marked by solid diamond in Fig. 2c).

To compare with the hardening from He bubbles, the hardening from irradiation-induced dislocation loops is taken into account. Based on a dispersed barrier hardening model [12], the increase in yield stress is equal to the increase in applied stress required to move a dislocation through a field of obstacles:

$$\Delta\sigma_y = \alpha M G b (N d)^{1/2} \quad (2)$$

where α is the barrier strength, 0.1 for loops; N is the loop density (m^{-3}) and d the loop diameter (nm). The density and diameter of small loops can be estimated from TEM and HRTEM images, as shown Fig. 2d. Take irradiated NC Mo5 and CG Mo0 as examples, the average loop densities are $1.5 \times 10^{22} m^{-3}$ and $1.9 \times 10^{24} m^{-3}$, and the average loop diameters are 2.0 nm and 5.8 nm, respectively. Thus, we can calculate the yield stress from Eq. (2) and obtain the hardness of 0.17 GPa and 3.37 GPa for irradiated NC Mo5 and CG Mo0, respectively. The hardness from both bubbles and loops for irradiated NC Mo5 and CG Mo0 are 0.38 and 3.98 GPa, respectively. Both are very close to the measured hardness increment (0.4 and 4.5 GPa) in Fig. 2c. It indicates that the additional hardening effect in irradiated Mo samples is mainly from the irradiation-induced dislocation loops and He bubbles.

As shown in Fig. 2c, the strong irradiation-induced hardening effect in ultra-fine-grained (UFG) or CG Mo (grain size > 90 nm) is mainly from the irradiation-induced dislocation loops. But as the grain size decreases into 90 nm, the irradiation-induced hardening decreases dramatically because both the density and the size of dislocation loops

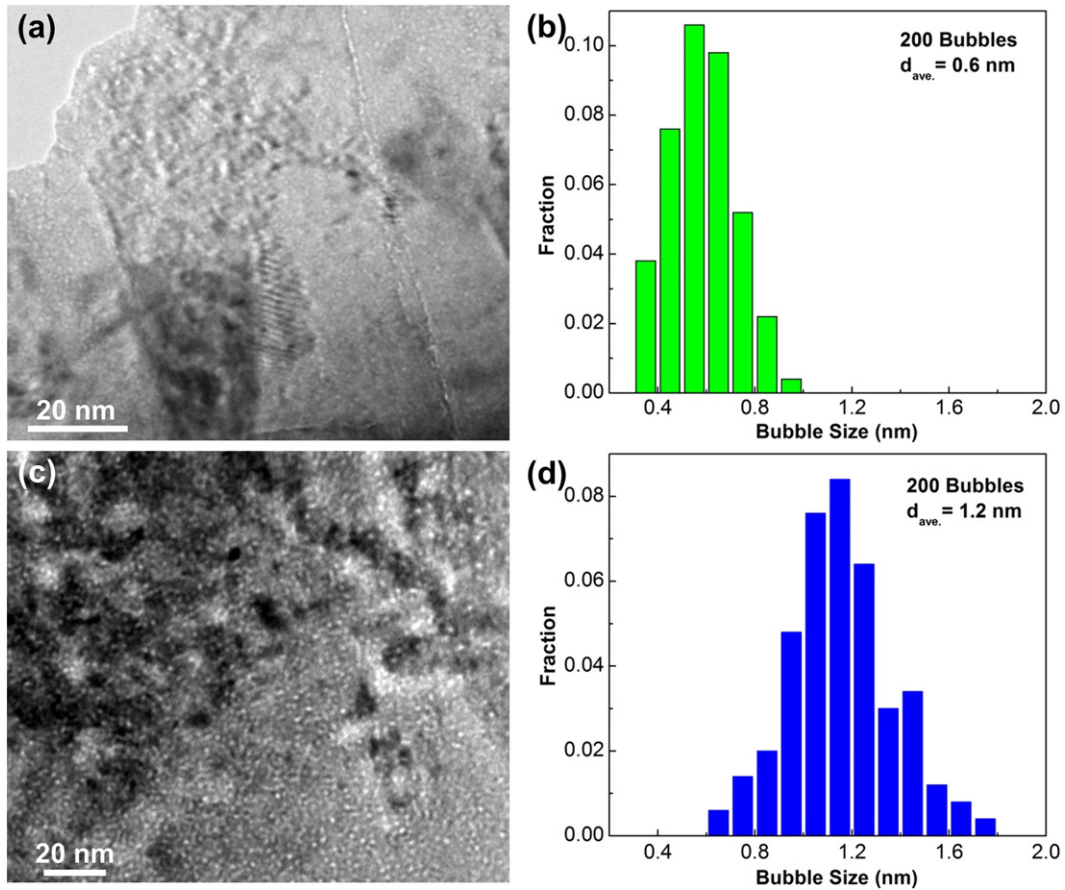


Fig. 3. TEM investigation of irradiation-induced He bubbles in NC Mo5 (a) and CG Mo0 (c) after He ion irradiation. (b, d) Bubble size distribution in NC Mo5 and CG Mo0 after irradiation, respectively.

and He bubbles decreases, especially the dramatic reduction of the density of the irradiation-induced dislocation loops. It should be noted that healing mechanism [37] may work in NC bcc metals under irradiation since interstitials released from GBs will help to annihilate the irradiation-induced defects such as vacancies and even decrease the density and the size of dislocation loops. And amounts of GBs in NC bcc metals can effectively act as sinks for He bubbles to reduce the negative effect of them [35]. Hence, the radiation tolerance of NC bcc metals will be well improved as the grain size decreases.

In summary, NC Mo shows much greater radiation resistance when the grain size is <90 nm than their UFG or CG counterparts. With decreasing grain size, the hardness increment of NC Mo after irradiation decreases and even reaches to zero at the grain size of 25 nm. This is because a low density and a small size of defects (dislocation loops and He bubbles) are produced in the grains smaller than 90 nm during irradiation.

Acknowledgement

This work was supported by the Laboratory Directed Research and Development program office of the Idaho National Laboratory. He ion implantation was supported by Center for Integrated Nanotechnologies, a DOE nanoscience user facility jointly operated by Los Alamos and Sandia National Laboratories. The authors wish to thank Dr. Dieter Wolf whose insight and discussions with the authors inspired and initiated the current study on bcc metals. The authors acknowledge the use of the Analytical Instrumentation Facility (AIF) at North Carolina State University, which is supported by the State of North Carolina and the National Science Foundation.

Appendix A. Supplementary data

Supplementary data to this article can be found online at <http://dx.doi.org/10.1016/j.scriptamat.2016.06.007>.

References

- [1] G. Ackland, *Science* 327 (2010) 1587–1588.
- [2] R.W. Grimes, R.J.M. Konings, L. Edwards, *Nat. Mater.* 7 (2008) 683–685.
- [3] U.S. DOE, A Technology Roadmap for Generation IV Nuclear Energy Systems Nuclear Energy Advisory Committee and the Generation IV International Forum, GIF-002-00, 2002.
- [4] R.W. Grimes, W.J. Nuttall, *Science* 329 (2010) 799–803.
- [5] T. Allen, J. Busby, M. Meyer, D. Petti, *Mater. Today* 13 (2010) 14–23.
- [6] E.M. Bringa, J.D. Monk, A. Caro, A. Misra, L. Zepeda-Ruiz, M. Duchaineau, F. Abraham, M. Nastasi, S.T. Picraux, Y.Q. Wang, D. Farkas, *Nano Lett.* 12 (2012) 3351–3355.
- [7] W. Xu, Y. Zhang, G. Cheng, W. Jian, P.C. Millett, C.C. Koch, S.N. Mathaudhu, Y. Zhu, *In-Situ Atomic-Scale Observation of Irradiation-Induced Void Formation*, *Nature Communications* 4, 2013.
- [8] I. Farnan, H. Cho, W.J. Weber, *Nature* 445 (2007) 190–193.
- [9] L.S. Novikov, V.N. Mileev, E.N. Voronina, L.I. Galanina, A.A. Makletsov, V.V. Sinolits, *J. Surf. Invest.: X-Ray, Synchrotron Neutron Tech.* 3 (2009) 199–214.
- [10] W.Z. Xu, Y.F. Zhang, G.M. Cheng, W.W. Jian, P.C. Millett, C.C. Koch, S.N. Mathaudhu, Y.T. Zhu, *Math. Res. Lett.* 2 (2014) 176–183.
- [11] G. Cheng, S. Yao, X. Sang, B. Hao, D. Zhang, Y.K. Yap, Y. Zhu, *Small* 12 (2016) 818–824.
- [12] G.S. Was, *Fundamentals of Radiation Materials: Metals and Alloys*, Springer, 2007.
- [13] B.D. Wirth, *Science* 318 (2007) 923–924.
- [14] N. Baluc, D.S. Gelles, S. Jitsukawa, A. Kimura, R.L. Klueh, G.R. Odette, B. van der Schaaf, J. Yu, *J. Nucl. Mater.* 367 (2007) 33–41.
- [15] N. Baluc, K. Abe, J.L. Boutard, V.M. Chernov, E. Diegele, S. Jitsukawa, A. Kimura, R.L. Klueh, A. Kohyama, R.J. Kurtz, R. Lasser, H. Matsui, A. Moslang, T. Muroga, G.R. Odette, M.Q. Tran, B. Van der Schaaf, Y. Wu, I. Yu, S.J. Zinkle, *Nucl. Fusion* 47 (2007) S696–S717.
- [16] E. Zarkadoulas, S.L. Daraszewicz, D.M. Duffy, M.A. Seaton, I.T. Todorov, K. Nordlund, M.T. Dove, K. Trachenko, *J. Phys. Condens. Matter* 25 (2013) 125402.

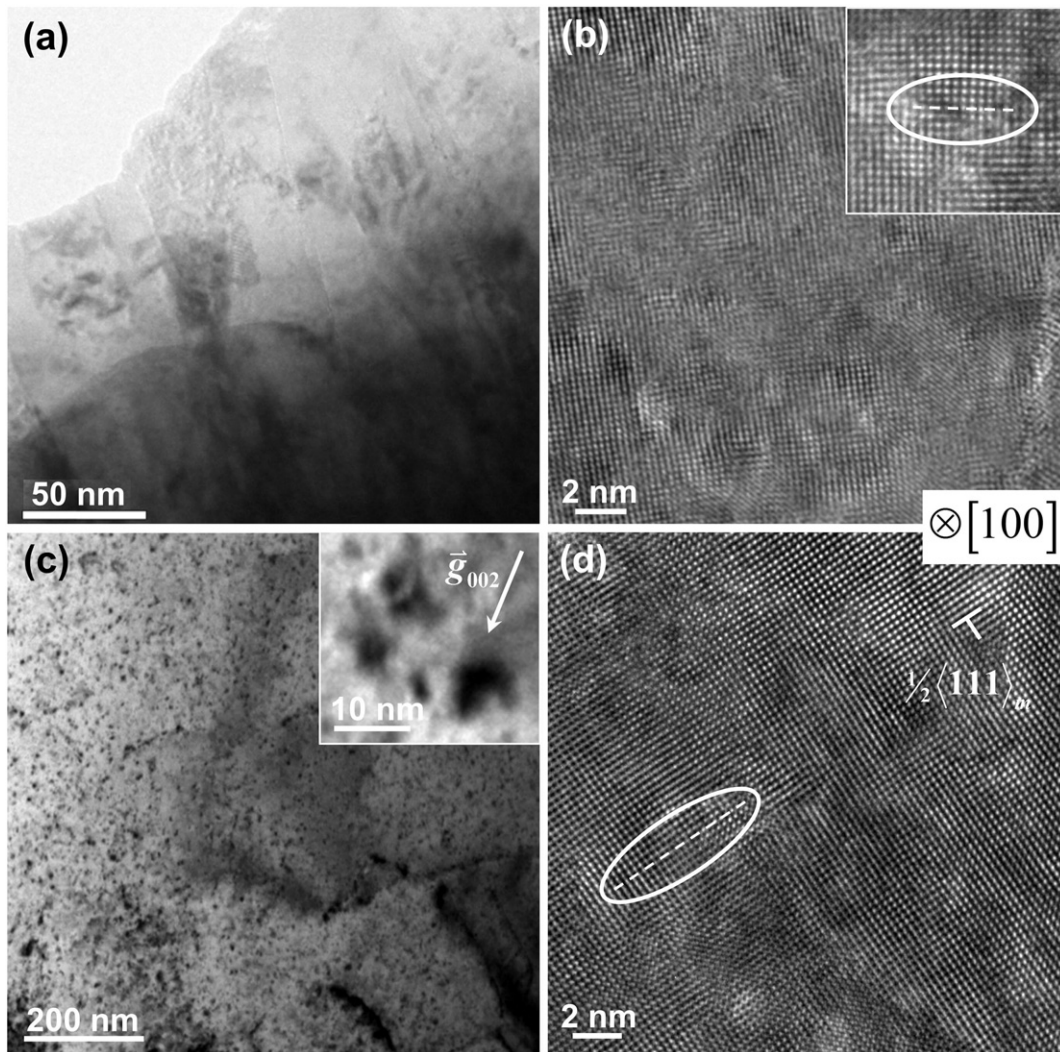


Fig. 4. TEM and HRTEM investigation of irradiation-induced defects (loops and dislocations) in NC Mo5 (a–b) and CG Mo0 (c–d) after He ion irradiation. Loops and mixed dislocations are marked in (d) and the inset in (b).

- [17] X. Tan, L. Luo, H. Chen, X. Zhu, X. Zan, G. Luo, J. Chen, P. Li, J. Cheng, D. Liu, Y. Wu, *Sci. Rep.* 5 (2015) 12755.
- [18] B. Beeler, M. Asta, P. Hosemann, N. Grønbech-Jensen, *J. Nucl. Mater.* 474 (2016) 113–119.
- [19] T.R. Allen, J. Gan, J.I. Cole, M.K. Miller, J.T. Busby, S. Shutthanandan, S. Thevuthasan, *J. Nucl. Mater.* 375 (2008) 26–37.
- [20] G.R. Odette, D.T. Hoelzer, *JOM* 62 (2010) 84–92.
- [21] S.J. Zinkle, N.M. Ghoniem, *Fusion Eng. Des.* 51–52 (2000) 55–71.
- [22] S. Ukai, M. Fujiwara, *J. Nucl. Mater.* 307 (2002) 749–757.
- [23] W. Xu, L. Li, M. Saber, C.C. Koch, Y. Zhu, R.O. Scattergood, *J. Nucl. Mater.* 452 (2014) 434–439.
- [24] K.Y. Yu, Y. Liu, C. Sun, H. Wang, L. Shao, E.G. Fu, X. Zhang, *J. Nucl. Mater.* 425 (2012) 140–146.
- [25] Y.T. Zhu, X.Z. Liao, X.L. Wu, *Prog. Mater. Sci.* 57 (2012) 1–62.
- [26] M.A. Meyers, A. Mishra, D.J. Benson, *Prog. Mater. Sci.* 51 (2006) 427–556.
- [27] Y.H. Zhao, T. Topping, J.F. Bingert, J.J. Thornton, A.M. Dangelewicz, Y. Li, W. Liu, Y.T. Zhu, Y.Z. Zhou, E.L. Lavermia, *Adv. Mater.* 20 (2008) 3028–3033.
- [28] X.L. Wu, Y.T. Zhu, Y.G. Wei, Q. Wei, *Phys. Rev. Lett.* 103 (2009).
- [29] G.M. Cheng, W.W. Jian, W.Z. Xu, H. Yuan, P.C. Millett, Y.T. Zhu, *Math. Res. Lett.* 1 (2013) 26–31.
- [30] Q. Zhou, J. Zhao, J.Y. Xie, F. Wang, P. Huang, T.J. Lu, K.W. Xu, *Mater. Sci. Eng. A* 608 (2014) 184–189.
- [31] G.M. Cheng, H. Yuan, W.W. Jian, W.Z. Xu, P.C. Millett, Y.T. Zhu, *Scr. Mater.* 68 (2013) 130–133.
- [32] Q.M. Wei, N. Li, N. Mara, M. Nastasi, A. Misra, *Acta Mater.* 59 (2011) 6331–6340.
- [33] N. Li, E.G. Fu, H. Wang, J.J. Carter, L. Shao, S.A. Maloy, A. Misra, X. Zhang, *J. Nucl. Mater.* 389 (2009) 233–238.
- [34] A. Misra, J.P. Hirth, R.G. Hoagland, *Acta Mater.* 53 (2005) 4817–4824.
- [35] A. Misra, M.J. Demkowicz, X. Zhang, R.G. Hoagland, *JOM* 59 (2007) 62–65.
- [36] M. Samaras, P.M. Derlet, H. Van Swygenhoven, M. Victoria, *Phys. Rev. Lett.* 88 (2002).
- [37] X.-M. Bai, A.F. Voter, R.G. Hoagland, M. Nastasi, B.P. Uberuaga, *Science* 327 (2010) 1631–1634.
- [38] Y. Zhang, P.C. Millett, M. Tonks, L. Zhang, B. Biner, *J. Phys. Condens. Matter* 24 (2012).
- [39] B.L. Eyre, D.M. Maher, R.C. Perrin, *J. Phys. F: Met. Phys.* 7 (1977) 1359–1369.
- [40] C.A. English, B.L. Eyre, S.M. Holmes, *J. Phys. F: Met. Phys.* 10 (1980) 1065–1080.
- [41] D.M. Maher, B.L. Eyre, *Philos. Mag.* 17 (1968) 1–6.
- [42] G.M. Cheng, W.Z. Xu, W.W. Jian, H. Yuan, M.H. Tsai, Y.T. Zhu, Y.F. Zhang, P.C. Millett, *J. Mater. Res.* 28 (2013) 1820–1826.
- [43] J. Friedel, *Philos. Mag.* 46 (1955) 1169–1186.
- [44] F. Kroupa, P.B. Hirsch, *Discuss. Faraday Soc.* 38 (1964) 49–55.